

## Article

# A Study on the Influence of Zr on the Strengthening of the Al-10% Al<sub>2</sub>O<sub>3</sub> Composite Obtained by Mechanical Alloying

Alexey S. Prosviryakov , Andrey I. Bazlov , Alexander Yu. Churyumov  and Anastasia V. Mikhaylovskaya

Department of Physical Metallurgy of Non-Ferrous Metals, National University of Science and Technology MISIS, Leninskiy Prospect 4, Moscow 119049, Russia; bazlov@misis.ru (A.I.B.); churyumov@misis.ru (A.Y.C.); mikhaylovskaya@misis.ru (A.V.M.)

\* Correspondence: prolex@misis.ru

**Abstract:** Al<sub>2</sub>O<sub>3</sub> is a traditional strengthening phase in aluminum matrix composites due to its high hardness and melting point. At the same time, zirconium is an important alloying element for heat-resistant aluminum alloys. However, its effect on the structure and properties of Al-Al<sub>2</sub>O<sub>3</sub> composites remains unexplored at present. In this work, the effect of the addition of Zr (5 wt%) on the microstructure and strengthening of the Al-10 vol% Al<sub>2</sub>O<sub>3</sub> composite was investigated for the first time. Composite materials with and without Zr addition were obtained through mechanical alloying as a result of ball milling for 20 h followed by multi-directional forging (MDF) at a temperature of 400 °C. OM, SEM and XRD were used to study the microstructure and its parameters. The work showed that the use of mechanical alloying and MDF contributes to the formation of dense composite samples with a nanocrystalline microstructure and a uniform distribution of alumina particles. The addition of Zr contributes to a 1.4-fold increase in the microhardness and yield strength of a compact sample at room temperature due to the formation of Al<sub>3</sub>Zr (L1<sub>2</sub>) dispersoids. It was been shown that the largest contribution to the strength of both materials comes from grain boundary strengthening, which is at least 50% of the yield strength. The resulting composites exhibit high heat resistance. For example, their compressive yield strength at 350 °C is approximately 220 MPa.

**Keywords:** mechanical alloying; aluminum matrix composites; Al-Al<sub>2</sub>O<sub>3</sub>; microstructure; microhardness; zirconium



**Citation:** Prosviryakov, A.S.; Bazlov, A.I.; Churyumov, A.Y.; Mikhaylovskaya, A.V. A Study on the Influence of Zr on the Strengthening of the Al-10% Al<sub>2</sub>O<sub>3</sub> Composite Obtained by Mechanical Alloying. *Metals* **2023**, *13*, 2008. <https://doi.org/10.3390/met13122008>

Academic Editor: Pengchao Kang

Received: 27 October 2023

Revised: 2 December 2023

Accepted: 7 December 2023

Published: 13 December 2023



**Copyright:** © 2023 by the authors. Licensee MDPI, Basel, Switzerland. This article is an open access article distributed under the terms and conditions of the Creative Commons Attribution (CC BY) license (<https://creativecommons.org/licenses/by/4.0/>).

## 1. Introduction

Traditional aluminum alloys can no longer meet the increased demands of modern products operating in harsh conditions. Important alloying elements for heat-resistant aluminum alloys are transition metals, such as zirconium [1–4]. However, their limiting solubility in aluminum is extremely low, which reduces the strengthening potential of the alloys. For the manufacturing of critical parts operating under extreme conditions, aluminum matrix composites can be used instead of aluminum alloys. Aluminum matrix composites have a number of advantages, including high strength properties at both ambient and elevated temperatures [5–11]. Traditional reinforcing phases in composites are ceramic particles, such as Al<sub>2</sub>O<sub>3</sub>, which are characterized by high hardness and melting temperatures [12]. Al-Al<sub>2</sub>O<sub>3</sub> composites are produced using various methods, including stir casting [13,14], gas pressure infiltration [15,16], ultrasonic casting [17,18], squeeze casting [19], semi-solid mechanical stirring [20], powder metallurgy [21] and mechanical alloying [22–31]. Mechanical alloying [32–37] is the most effective method for forming a homogeneous ultrafine structure. This method makes it possible to achieve a uniform distribution of reinforcing particles in a metal matrix as a result of alternating processes of welding and the destruction of powder particles of processed materials during ball milling. At the same time, the severe plastic deformation that accompanies the mechanical alloying process leads to the formation of a nanocrystalline structure that provides high strength properties.

Zebarjad and Sajjadi [25] showed that increasing the milling time of the Al-5%Al<sub>2</sub>O<sub>3</sub> composite during mechanical alloying results in the formation of fine alumina particles and their uniform distribution within the aluminum matrix. Increasing the milling time in the steady state has no significant effect on their size distribution within the aluminum. In another work [26], these authors showed that the mechanical and physical properties of milled Al-5 wt% Al<sub>2</sub>O<sub>3</sub> composites depend on the milling time. Thus, an increase in the milling time leads to an increase in electrical resistivity, microhardness, compressive strength and wear resistance with a simultaneous decrease in ductility. However, in the steady state, increasing the milling time does not have a significant effect on the properties. Toozandehjani et al. [27] also investigated the effect of the milling time on the morphology, microstructure and physical and mechanical properties of Al-5 wt% Al<sub>2</sub>O<sub>3</sub>. It was shown that increasing the milling time leads to a homogeneous dispersion of Al<sub>2</sub>O<sub>3</sub> nanoparticles, a decrease in their clustering and interparticle spacing and a reduction in the size of the powder particles. In addition, ball milling contributes to crystalline refinement and the accumulation of internal stresses due to intense plastic deformation. These morphological and microstructural changes of composite powders caused by increasing the milling time contribute to the improvement of density, densification, microhardness, nanohardness and Young's modulus of Al-5Al<sub>2</sub>O<sub>3</sub> nanocomposites. Poirier et al. [28] successfully prepared Al nanocomposites using Al<sub>2</sub>O<sub>3</sub> particles of different sizes with contents up to 10 vol%. The microhardness of a 10% composite powder was shown to be almost five times higher than that of pure unground aluminum. Reducing the Al<sub>2</sub>O<sub>3</sub> particle size from 400 to 4 nm increases the microhardness of the composite powder by 11%. Wagih [29] investigated the effect of different weight fractions of alumina (0, 2.5, 5 and 10 wt%) on the microstructure and strength of Al/Al<sub>2</sub>O<sub>3</sub> composites obtained through mechanical alloying. The results showed that the addition of alumina particles accelerated the milling process, resulting in higher work hardening rates, refinement of the composite powder particles and improvements in their morphology. Increasing the mass fraction of reinforcing nano-sized Al<sub>2</sub>O<sub>3</sub> particles results in their more uniform distribution in the Al matrix. The mechanical properties of the composite increase with an increasing alumina content. Tavoosi et al. [30] investigated the wear properties of Al nanocomposites containing different amounts of nanosized Al<sub>2</sub>O<sub>3</sub> particles (4, 8, 12 and 16 wt%) in dry sliding tests. The results showed that hardness and wear resistance increased with an increasing Al<sub>2</sub>O<sub>3</sub> content of the nanocomposites. The predominant wear mechanisms in the Al-Al<sub>2</sub>O<sub>3</sub> system are adhesion and delamination with lower and higher Al<sub>2</sub>O<sub>3</sub> contents, respectively. Razavi Tousi et al. [31] studied the particle size, morphology and compressibility of Al-20 wt% Al<sub>2</sub>O<sub>3</sub> composite powder as a function of milling time. It was shown that the addition of alumina particles reduces the time required to reach the steady state where the distribution of particles in the Al matrix is completely homogeneous. This makes it possible to increase the hardness of the composite through the formation of a nanocrystalline metal matrix and dispersion reinforcement mediated by oxide particles.

In general, Al-Al<sub>2</sub>O<sub>3</sub> composites have been well studied. In addition to alumina, transition metals, such as zirconium, can improve the strength properties of aluminum materials at room and elevated temperatures through the formation of the strengthening intermetallic particles Al<sub>3</sub>Zr. The Al<sub>3</sub>Zr (L1<sub>2</sub>) phase is an effective aluminum hardener and anti-crystallization agent in Al alloys [38]. Al-Aqeeli et al. [39] developed Al-Mg-Zr nanocomposite materials through the mechanical alloying of elemental powders. He showed that when Zr is added (up to 35 at.%) to the Al-Mg alloy, a solid solution and an intermetallic is formed, resulting in structural stability and an increase in hardness. Muthaiah et al. [40] studied the extension of the solid solubility of Zr (1–10 at.%) in Al through mechanical alloying and the thermal stability of prepared Al-Zr materials. It was shown that a nanocrystalline solid solution is formed during ball milling. The formation of an Al<sub>3</sub>Zr intermetallic phase played an important role in stabilizing the nanocrystalline grains. Srinivasarao et al. [41] used Zr and Al<sub>3</sub>Zr powders to develop mechanically alloyed Al-Zr nanocomposite alloys. The alloys, after spark plasma sintering,

consisted of Al with nano-sized grains and a finely dispersed  $\text{Al}_3\text{Zr}$  ( $\text{L}_{12}$ ) phase due to which these nanocomposites exhibited a high compressive strength of 1 GPa with 10% plasticity. In our previous work [42], we investigated the effect of the Zr content (5–20 wt%) on the strengthening of composites based on an Al-Cu-Mn alloy. It was shown that mechanical alloying leads to an increase in the solubility of zirconium in aluminum up to 20 wt%. When the Zr content increases, the microhardness of hot-pressed samples increases to 520 HV due to precipitation hardening and the formation of a metastable  $\text{Al}_3\text{Zr}$  ( $\text{L}_{12}$ ) phase. The compact samples exhibited high strength at room and elevated temperatures. Kaveendran et al. [43] synthesized in situ hybrid ( $\text{Al}_3\text{Zr} + \text{Al}_2\text{O}_3$ )/2024 aluminum matrix composites using low-energy ball milling and reactive hot pressing. With a total reinforcement content of 10 vol%, the synthesised  $\text{Al}_3\text{Zr}$  and  $\text{Al}_2\text{O}_3$  particles had effectively reinforced the Al matrix.

In general, the effect of transition metals and intermetallic compounds on the structure and properties of Al- $\text{Al}_2\text{O}_3$  composites has not been well studied. These different reinforcement phases may have a synergistic effect on the properties of the aluminum matrix composite. Therefore, the aim of this work was to investigate the effect of zirconium addition on the microstructure and strengthening of the Al- $\text{Al}_2\text{O}_3$  composite.

## 2. Materials and Methods

In this work, Al-10 wt%  $\text{Al}_2\text{O}_3$  composites with and without the addition of 5 wt% Zr were investigated to compare their microstructure and mechanical properties. The starting components were Al and  $\text{Al}_2\text{O}_3$  powders (average particle size of about 500 nm) and zirconium chips of several millimeters in size. Stearic acid was added at 2 wt% to the material without Zr addition to prevent welding. The starting materials were processed in a Retsch PM400 planetary ball mill in an argon atmosphere at a speed of 300 rpm. The ball-to-powder weight ratio was 20:1. The milling time was 20 h. To study the morphology, the composite granules were mixed with acrylic powder in a holder and impregnated with a monomer liquid. The samples obtained after curing were subjected to grinding and polishing. The morphology of the granules and the microstructure were studied using a TESCAN VEGA 3LMH scanning electron microscope. Microhardness was measured using the Vickers method on a 402MVD instrument at a load of 50 g, as an average of 10 measurements. XRD analysis was performed using a D8 Discover diffractometer (Bruker-AXS) with  $\text{CuK}\alpha$  radiation.

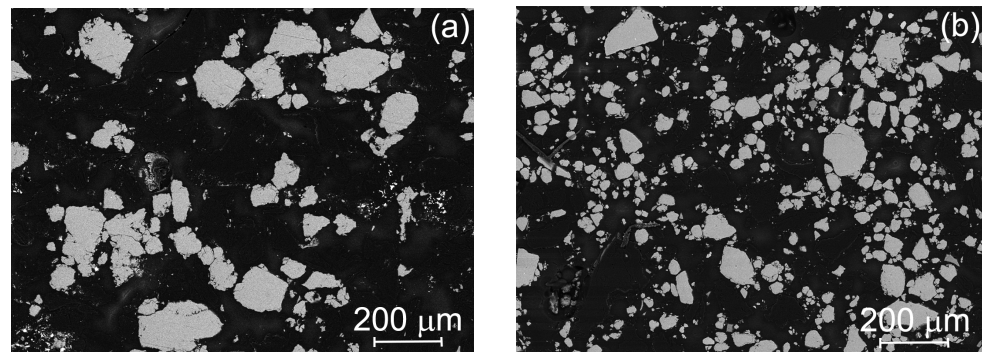
The composite powders were precompressed through hot pressing at a temperature of 350 °C and a pressure of 400 MPa in a steel matrix with a rectangular hole. The samples obtained had the shape of a parallelepiped with dimensions of  $9 \times 9 \times 18$ . Multidirectional forging (MDF) was then carried out at 400 °C. The specimen was placed vertically in the same die and deformed to a value of  $e = 0.8$  of the true strain at a cross-head velocity of 5 mm/min, corresponding to an initial strain rate of  $5 \times 10^{-3} \text{ s}^{-1}$ . Deformation occurred along two of the three axes, and the geometry of the specimen remained constant after each pass. In order to work out all the axes of deformation in the specimen after each pass, the specimen was rotated 90° from its original position after each operation. Three passes with two rotations constituted one forging cycle. In total, 6 passes or 2 complete deformation cycles were performed with a cumulative strain of  $\sum e = 4.8$ . A detailed scheme of specimen rotation during isothermal multidirectional forging is presented in [44].

The density of the compacted samples was measured via hydrostatic weighing. Compression tests were performed on a Zwick Z250 universal testing machine at a temperature of 350 °C with an initial strain rate of  $10^{-3} \text{ s}^{-1}$ .

## 3. Results and Discussion

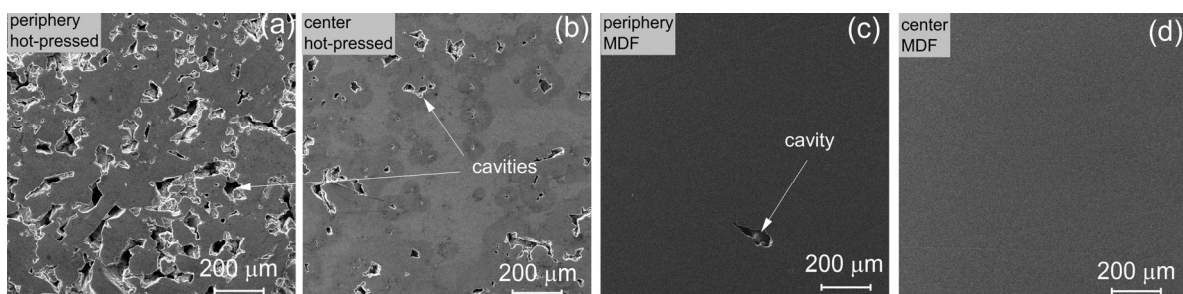
Figure 1 shows images of powder particles (granules) of the composites studied in the plane of the section after mechanical alloying. These granules were formed through repeated alternating processes of welding and the destruction of powder particles during milling as a result of severe plastic deformation. These processes take place under the

impact and abrasion of the milling balls. From Figure 1a, it can be seen that the edges of the Al-10% Al<sub>2</sub>O<sub>3</sub> granules were uneven and their size was about 100 μm. At the same time, with the addition of 5 wt% Zr, the shape of the granules became more regular and their average size decreased to about 40 μm, indicating the development of greater work hardening in this material and the predominance of the destruction mechanism.



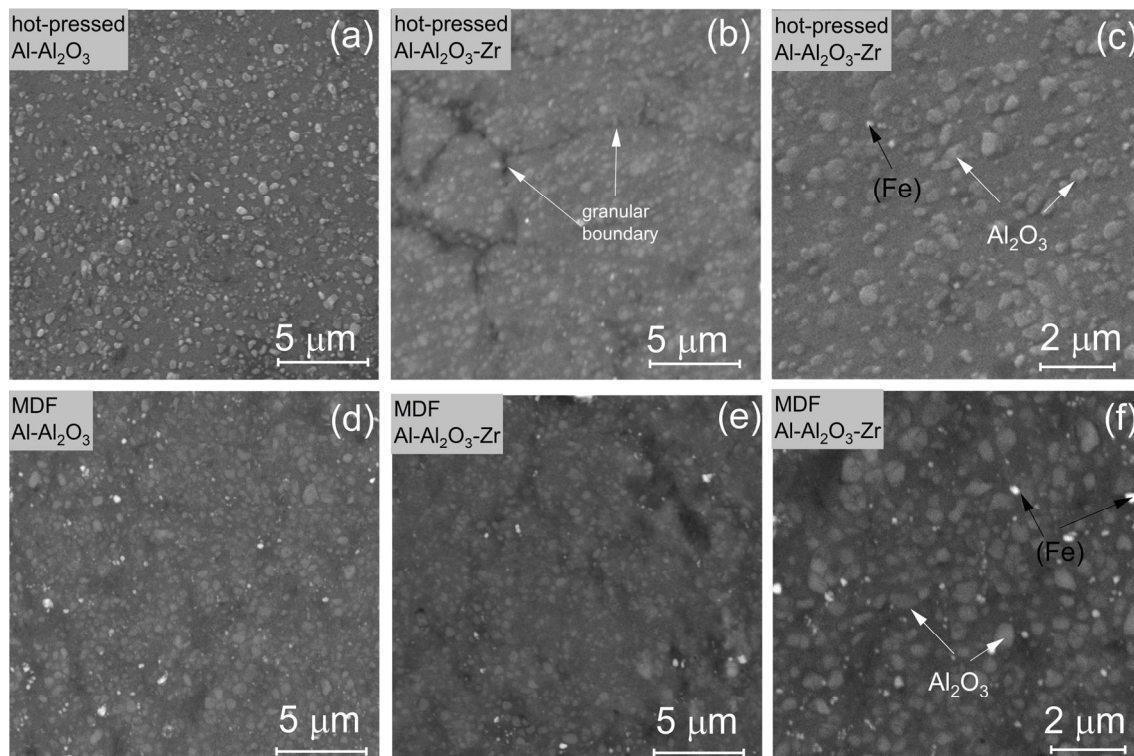
**Figure 1.** Morphology of granules of (a) Al-10%Al<sub>2</sub>O<sub>3</sub> and (b) Al-10%Al<sub>2</sub>O<sub>3</sub>-5%Zr composites after 20 h of milling.

The residual porosity was significantly higher at the surface of the samples after hot pressing for both alloys studied, while a high porosity was defined at the periphery of the samples and a smaller fraction in the center (the example for the Al-10%Al<sub>2</sub>O<sub>3</sub>-5%Zr material is shown in Figure 2a,b). At high magnification, the boundaries between the granules were observed (Figure 3b). The subsequent MDF resulted in a strong decrease in porosity and discontinuities along the granule boundaries in both the central and peripheral parts of the samples (Figure 2c,d and Figure 3d,e), indicating the increase in sample quality. Meanwhile, some residual discontinuities were detected in the Zr-bearing material. The porosity reduction also supports the density change analysis. The density of the samples increased from 2.47 to 2.73 g/cm<sup>3</sup> and from 2.69 to 2.81 g/cm<sup>3</sup> for samples without Zr and with Zr addition, respectively.



**Figure 2.** Porosity of Al-10%Al<sub>2</sub>O<sub>3</sub>-5%Zr after hot pressing (a,b) and MDF (c,d) at the periphery (a,c) and center (b,d).

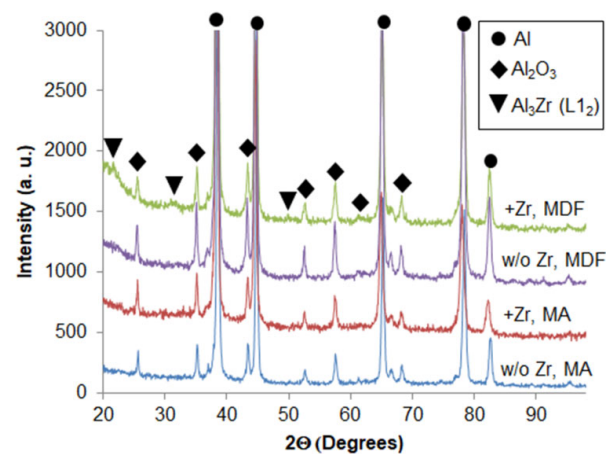
The microstructure of both materials showed light gray Al<sub>2</sub>O<sub>3</sub> particles uniformly distributed in the aluminum matrix (Figure 3). The average size of the ceramic particles was about 400 nm. Their distribution was independent of the material composition and accumulated strain. The white inclusions were impurity iron particles introduced into the material through the abrasion of steel grinding balls during mechanical alloying.



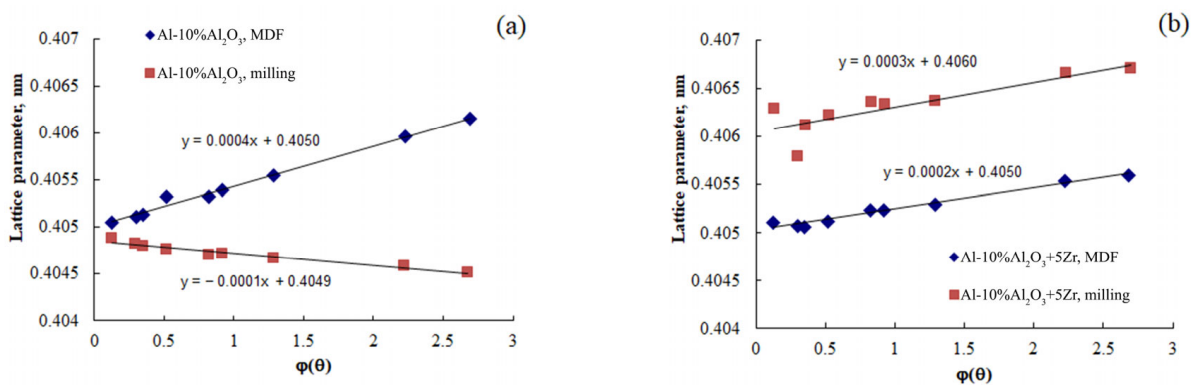
**Figure 3.** Microstructure of Al-10%Al<sub>2</sub>O<sub>3</sub> (a,d) and Al-10%Al<sub>2</sub>O<sub>3</sub>-5%Zr (b,c,e,f) compact specimens after hot pressing (a–c) and forging (d–f) at different magnifications.

Figure 4 shows the X-ray diffraction patterns of the Al-10%Al<sub>2</sub>O<sub>3</sub> and Al-10%Al<sub>2</sub>O<sub>3</sub>-5%Zr composites in the as-milled state and after forging. The XRD analysis of both materials showed the presence of Al<sub>2</sub>O<sub>3</sub> phase lines in all two states. At the same time, after mechanical alloying, there were no zirconium lines in the Al-10%Al<sub>2</sub>O<sub>3</sub>-5%Zr material, and the lattice parameter of Al increased from 0.4049 to 0.406 nm compared to the Al-10%Al<sub>2</sub>O<sub>3</sub> powder, as shown in Figure 5. The lattice parameters were calculated using the Nelson-Riley extrapolation function [45]:

$$a = \varphi(\theta) = \frac{1}{2} \left( \frac{\cos^2 \theta}{\sin \theta} + \frac{\cos^2 \theta}{\theta} \right) \quad (1)$$



**Figure 4.** X-ray diffraction patterns of the studied materials after mechanical alloying and after forging.



**Figure 5.** The Nelson–Riley plots for (a) Al-10%Al<sub>2</sub>O<sub>3</sub> and (b) Al-10%Al<sub>2</sub>O<sub>3</sub>-5%Zr composites.

The disappearance of the Zr lines and an increase in the lattice parameter (the atomic radius of Zr is greater than the atomic radius of Al) indicated the dissolution of zirconium in aluminum as a result of high-energy milling due to the activation of diffusion processes with intense plastic deformation. The obtained value of the parameter corresponded to the complete dissolution of 5 wt% Zr [42]. This solubility was almost 5 times higher than the values obtained using traditional casting methods [46].

After forging, the lattice parameter of the material with the addition of zirconium was restored to the value corresponding to pure aluminum, while for the material without zirconium, the parameter did not change after hot deformation, as can be seen from Figure 5. The decrease in the lattice parameter in the Al-10%Al<sub>2</sub>O<sub>3</sub>-5%Zr material is explained by the decomposition of the supersaturated solid solution with the precipitation of the non-equilibrium phase Al<sub>3</sub>Zr (L1<sub>2</sub>) of the cubic modification, for which lines were visible in the diffraction pattern (Figure 4). These dispersoids were small in size (5–20 nm) [47] and were therefore not detectable in the microstructure in Figure 3.

It should also be noted that in all but one case, the slope of the extrapolation line in Figure 5 was positive. However, for the Al-10%Al<sub>2</sub>O<sub>3</sub> material in the as-milled state, this slope was negative, and it was associated with a decrease in interplanar spacing. This may be due to compressive deformation of the crystal lattice as a result of severe plastic deformation during the milling process. For the Al-10%Al<sub>2</sub>O<sub>3</sub>-5%Zr material, this phenomenon is likely to be compensated for by an increase in interplanar spacing due to the dissolution of zirconium, and hence, the line slope is positive for this material.

The formation of a highly deformed structure during mechanical alloying was confirmed through X-ray diffraction analysis. Figure 6 shows the Williamson–Hall plots plotted using equation [48]:

$$\beta_{hkl} \cos \theta = \frac{K\lambda}{D} + 4\varepsilon \sin \theta \quad (2)$$

where  $\beta$  is an integral broadening of the diffraction peak,  $\theta$  is the Bragg angle,  $K$  is the shape factor (0.9),  $\lambda$  is the wavelength of CuK $\alpha$  radiation (0.154 nm),  $D$  is the mean crystallite size and  $\varepsilon$  is the microstrain.

In this figure, the slope of the straight line can be used to determine the microstrain of the aluminum matrix, and the average size of the crystallites (grains) can be determined from the point of intersection with the vertical axis. The crystallite size determined by the W-H method was in good agreement with the grain size determined via TEM [9]. This figure shows that the microstrain values of both materials studied after milling were around 0.2%, which corresponds to a highly deformed structure. It can also be seen from Figure 6a that for the Al-10%Al<sub>2</sub>O<sub>3</sub> material, the slope after forging increased significantly compared to the state after milling, which was associated with an even greater increase in microstrain from 0.002 to 0.0029 and an increase in crystallite size from 52 to 80 nm. An increase in the microstrain after hot deformation can be caused by thermal stresses during cooling due to the difference in thermal expansion coefficients between aluminum and Al<sub>2</sub>O<sub>3</sub>.

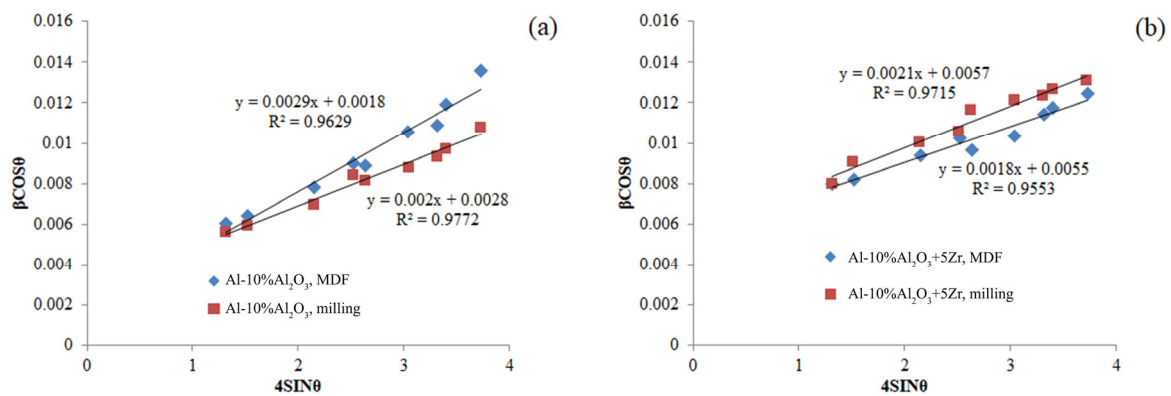


**Figure 6.** The Williamson–Hall plots for (a) Al-10%Al<sub>2</sub>O<sub>3</sub> and (b) Al-10%Al<sub>2</sub>O<sub>3</sub>-5%Zr composites.

However, as can be seen from Figure 6b, the microstrain determined from the corresponding slope of the line for the material with zirconium addition slightly decreased from 0.21 to 0.18% and the crystallite size also changed slightly (from 25 to 28 nm). It should be noted that the crystallite size of the aluminum matrix in the Al-10%Al<sub>2</sub>O<sub>3</sub>-5%Zr material was significantly smaller, which is related to the anti-recrystallization effect of zirconium. In the Al-10%Al<sub>2</sub>O<sub>3</sub> material, there was no such additive, and therefore, the recrystallization processes were more pronounced, which is reflected by the coarsening of the crystallites. A slight decrease in the microstrain in the Al-10%Al<sub>2</sub>O<sub>3</sub>-5%Zr material may be due to the release of microstresses generated by the dissolution of Zr as a result of the decomposition of the supersaturated Al solid solution.

It is known that a change in the microstructure leads to a change in the mechanical properties. Thus, the microhardness of the material with Zr addition after forging decreased from  $285 \pm 9$  to  $244 \pm 13$  HV compared to the as-milled state. The reason for this decrease may be due to the decomposition of the solid solution, as the effect of solid solution strengthening in this case was greater than the effect of dispersion strengthening [42]. However, the microhardness of the Al-10%Al<sub>2</sub>O<sub>3</sub> material did not change significantly after forging and was  $176 \pm 8$  HV, while after milling, it was  $175 \pm 12$ . The lack of a change in microhardness may be due to the softening caused by grain growth being compensated for by microstrains. In general, the addition of zirconium increased the microhardness of the forged samples by 70 HV.

In order to evaluate the influence of the different contributions to the strengthening of Al-10%Al<sub>2</sub>O<sub>3</sub> materials with and without Zr addition, the corresponding calculations were carried out using the following equation:

$$\sigma = \sigma_0 + \sigma_{GB} + \sigma_{Dis} + \sigma_{Or} \quad (3)$$

where  $\sigma$  is the yield strength of the composite material,  $\sigma_0$  is the Peierls–Nabarro stress (10 MPa for Al),  $\sigma_{GB}$  is the grain-boundary strengthening,  $\sigma_{Dis}$  is the dislocation strengthening and  $\sigma_{Or}$  is the Orowan strengthening.

Grain boundaries are known to be effective barriers to dislocation movement. Dislocations are restrained at boundaries and form clusters. Elastic stress fields are generated around them, acting on the boundaries and adjacent areas of neighboring grains, in addition to the externally applied stresses. Grain boundary strengthening is calculated using the Hall–Petch equation [49]:

$$\sigma_{GB} = kD^{-1/2} \quad (4)$$

where  $k$  is the Hall–Petch coefficient that is equal to 0.1 and  $D$  is the grain size.

As calculated using the Williamson–Hall method, the crystallite (grain) size for materials without and with added zirconium was 80 and 28 nm, respectively. Substituting these values, we find that the values of the contribution of grain boundary strengthening to

the yield strength of forged Al-10%Al<sub>2</sub>O<sub>3</sub> and Al-10%Al<sub>2</sub>O<sub>3</sub>-5%Zr specimens are 364 and 608 MPa, respectively.

Clusters of dislocations formed during plastic deformation create elastic stress fields around themselves that block dislocation sources. As a result, the stress required to continue deformation and for dislocations to bypass the existing barriers increases. The contribution of strengthening due to the dislocation forest is calculated using the Taylor equation:

$$\sigma_{Dis} = M\alpha Gb\rho^{1/2} \quad (5)$$

where  $M$  is the Taylor factor equal to 3.06,  $\alpha$  is a dimensionless constant related to the dislocations interaction (0.3 for Al),  $G$  is the shear modulus (26 GPa for Al),  $b$  is the Burgers vector (0.286 nm for Al) and  $\rho$  is the dislocation density, which is calculated using the following equation [50]:

$$\rho = \frac{n\varepsilon}{Db} \quad (6)$$

where  $n$  is the coefficient (~7 for fcc metal).

Using the values of microstrain and average crystallite size calculated using Equation (2), we found that the contribution from the dislocation strengthening of Al-10%Al<sub>2</sub>O<sub>3</sub> and Al-10%Al<sub>2</sub>O<sub>3</sub>-5%Zr is 143 and 191 MPa, respectively.

Closely spaced dispersed particles also contribute to strengthening through the Orowan mechanism, where dislocations are pushed between them to form loops. The strengthening contribution in this case was estimated using the following equation [51]:

$$\sigma_{Or} = \frac{0.13Gb}{\lambda} \ln\left(\frac{d}{2b}\right) \quad (7)$$

where  $d$  is the average particles size (400 nm for Al<sub>2</sub>O<sub>3</sub> and 20 nm for Al<sub>3</sub>Zr) and  $\lambda$  is the interparticle distance, which is calculated using the following formula:

$$\lambda = d \left[ \left( \frac{1}{2V} \right)^{1/3} - 1 \right] \quad (8)$$

where  $V$  is the volume fraction of strengthening particles (0.1 for Al<sub>2</sub>O<sub>3</sub> and 0.06% for Al<sub>3</sub>Zr [34]. For the material with the zirconium addition, the values of  $\lambda$  and  $\sigma_{Or}$  were calculated separately for Al<sub>2</sub>O<sub>3</sub> and Al<sub>3</sub>Zr. As a result of the calculations, the values of the contribution of strengthening caused by dispersed particles for Al-10%Al<sub>2</sub>O<sub>3</sub> and Al-10%Al<sub>2</sub>O<sub>3</sub>-5%Zr materials were 22 and 189 MPa, respectively. It can be seen here that nanosized Al<sub>3</sub>Zr dispersoids have the greatest strengthening effect compared to submicron Al<sub>2</sub>O<sub>3</sub> particles.

The values of the contributions of the various factors and the values of the yield strength calculated using Equation (3) for the materials studied are summarized in Table 1. Estimates of the yield stress obtained using the Tabor equation [52] are also shown:

$$\sigma^{HV} = \frac{9.8HV}{3} \quad (9)$$

where  $HV$  is the hardness value in kgf/mm<sup>2</sup>.

**Table 1.** Comparison of different hardening contributions and calculated yield stress values for Al-10%Al<sub>2</sub>O<sub>3</sub> and Al-10%Al<sub>2</sub>O<sub>3</sub>-5%Zr composites after forging.

Material	$\sigma_{GB}$ , MPa		$\sigma_{Dis}$ , MPa	$\sigma_{Or}$ , MPa	$\sigma$ , MPa		$\sigma^{HV}$ , MPa
	$k = 0.1$	$k = 0.07$			$k = 0.1$	$k = 0.07$	
Al-10%Al <sub>2</sub> O <sub>3</sub>	354	—	143	22	529	—	572
Al-10%Al <sub>2</sub> O <sub>3</sub> -5%Zr	598	418	191	189	988	808	823

As can be seen from this table, the calculated values of the yield strength for the material Al-10%Al<sub>2</sub>O<sub>3</sub>, obtained using Equation (3), turned out to be lower than the value estimated using Equation (9). The reason for this difference may be that the following effect was not considered in the calculation of the contribution of the dispersed particles to the strengthening. As a result of the decomposition of stearic acid, carbon in the aluminum matrix can be released to form hard-to-detect hardening aluminum carbide dispersoids, which make an additional contribution to Orowan strengthening [9]. At the same time, the stress value for the Al-10%Al<sub>2</sub>O<sub>3</sub>-5%Zr composite, obtained from Equation (3) using a Hall–Petch coefficient of 0.1, was significantly higher than the value estimated from microhardness. This can be the reason that at extremely small grain sizes, the slope of the Hall–Petch relationship decreases due to a transition from dislocation-based deformation to grain boundary sliding [53]. The use of the Hall–Petch coefficient value of 0.07 obtained from fitting in Equation (4) resulted in a lower stress value, which was almost the same as that obtained using the Tabor equation. Table 1 also shows that the largest contribution to the yield strength of composites was made by grain boundary strengthening, ranging from 52 to 65%. At the same time, the strength of the material with the addition of zirconium exceeded the strength of the material without zirconium by 1.4 times, due to the strengthening effect of Al<sub>3</sub>Zr dispersoids.

Compression diagrams for compact samples obtained after hot pressing and MDF are shown in Figure 7. It can be seen that the compression curves for the forged samples were significantly higher than those for the pressed samples. This indicates that forging results in a significant increase in strength compared to pressing, due to a higher degree of densification. Meanwhile, the ductility of the Zr-added material was slightly lower than that of the Al-10%Al<sub>2</sub>O<sub>3</sub> material. This may be due to the retention of discontinuities in the microstructure due to the higher microhardness of the powder and smaller particle size. It should also be noted that although the microhardness and calculated yield strength at room temperature were higher for the Al-10%Al<sub>2</sub>O<sub>3</sub>-5%Zr material compared to Al-10%Al<sub>2</sub>O<sub>3</sub>, the yield strength at 350 °C was approximately the same for both materials and was approximately 220 MPa, which is a very high heat resistance index. It is evident that the alumina particles, which are inert to the metal matrix, make a significant contribution to the creep strength compared to the inhibition of dislocation motion at room temperature. In addition, high temperature strength is achieved with a grain size of less than 100 nm, indicating that there is no contribution from diffusion creep. The lack of a difference in the yield strength may be due to the fact that in the first material, due to the very small grain size, deformation can occur in the initial phase at elevated temperatures through grain boundary sliding, whereas in the second material, the dislocation strengthening mechanism is mainly involved.

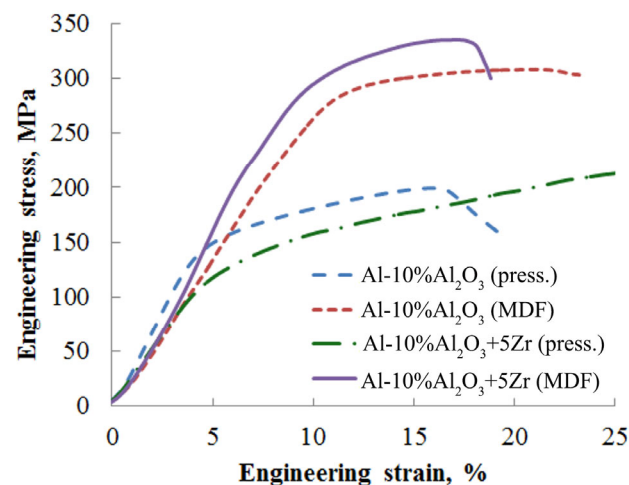
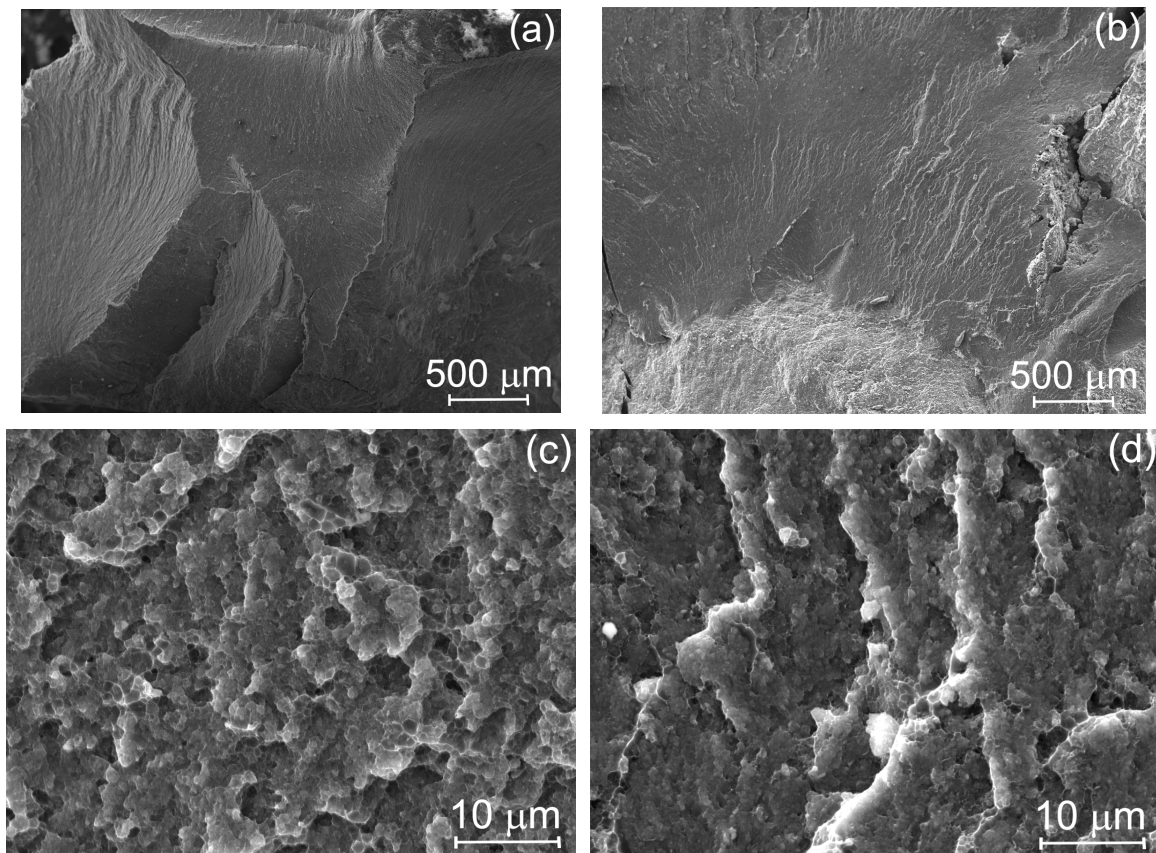


Figure 7. Compression curves of the studied composites at 350 °C.

Figure 8 shows the fractographs of the forged specimens after compression testing. At low magnification (Figure 8a,b), a flat fracture surface with traces of plastic deformation can be seen for both materials, indicating a predominantly brittle fracture pattern. However, at a higher magnification (Figure 8c,d), the fracture surface showed a dimpled structure characteristic of ductile fracture. The size of the pits was on the order of 1  $\mu\text{m}$ . They appeared to have been formed through the detachment of alumina particles from the Al matrix. In the Al-10%Al<sub>2</sub>O<sub>3</sub> material, the dimpled structure was more homogeneous than in the Zr-containing material due to a smaller number of defects (larger size of the initial granules). This explains the lower ductility of the latter. Based on the analysis of the presented fractographic images, it can be assumed that brittle fracture along the discontinuities is preceded by ductile fracture within the initial granules.



**Figure 8.** Fractographs of (a,c) Al-10%Al<sub>2</sub>O<sub>3</sub> and (b,d) Al-10%Al<sub>2</sub>O<sub>3</sub>-5%Zr forged composites after compression tests at different magnifications: (a,b) low magnification, (c,d) high magnification.

#### 4. Conclusions

The work has shown that high energy ball milling of materials the Al-10 vol% Al<sub>2</sub>O<sub>3</sub>/+5 wt% Zr for 20 h followed by multi-directional forging at 400 °C results in the formation of dense composite samples with a nanocrystalline microstructure and uniform distribution of Al<sub>2</sub>O<sub>3</sub> particles. At the same time, the addition of 5 wt% Zr contributes to a 1.4-fold increase in the microhardness and yield strength of a compact sample at room temperature. Estimates of various possible contributions indicate that this increment is due to the strengthening effect of the Al<sub>3</sub>Zr (L1<sub>2</sub>) dispersoids precipitated from the supersaturated solid solution of zirconium in aluminum formed during the milling process. It has also been shown that the largest contribution to the strength of both materials comes from grain boundary strengthening, which is at least 50% of the yield strength. In addition, the compressive yield strength of the composites studied at 350 °C is about 220 MPa, which demonstrates their high heat resistance.

**Author Contributions:** Conceptualization, A.S.P. and A.V.M.; methodology, A.S.P. and A.I.B.; software, A.S.P.; validation, A.S.P.; formal analysis, A.S.P.; investigation, A.S.P., A.I.B. and A.V.M.; resources, A.V.M.; data curation, A.S.P.; writing—original draft preparation, A.S.P.; writing—review and editing, A.S.P.; visualization, A.S.P.; supervision, A.S.P.; project administration, A.I.B., A.V.M. and A.Y.C.; funding acquisition, A.I.B., A.V.M. and A.Y.C. All authors have read and agreed to the published version of the manuscript.

**Funding:** This work was funded by the Ministry of Science and Higher Education in a framework of the State Task to MISIS University, project code of FSME-2023-0005. SEM investigations were carried out with the financial support of the Strategic Academic Leadership Program “Priority 2030” (project K2-2022-001).

**Data Availability Statement:** The data presented in this study are available on request from the corresponding author. The data are not publicly available due to privacy reasons.

**Acknowledgments:** The authors are grateful to V.V. Cheverikin for fractographic analysis.

**Conflicts of Interest:** The authors declare no conflict of interest.

## References

1. Czerwinski, F. Thermal Stability of Aluminum Alloys. *Materials* **2020**, *13*, 3441. [\[CrossRef\]](#)
2. Deng, S.-X.; Li, J.-F.; Ning, H.; Lu, D.-D.; Zeng, G.-J.; Liu, Z.-Z.; Xiang, H.; Que, J.-R.; Liu, D.-Y. Effect of Zr addition on the microstructure evolution and mechanical properties of extruded Al–Cu–Li–Mn alloys. *Mater. Charact.* **2023**, *202*, 113011. [\[CrossRef\]](#)
3. Yang, Y.; Tan, P.; Sui, Y.; Jiang, Y.; Zhou, R. Influence of Zr content on microstructure and mechanical properties of As-cast Al–Zn–Mg–Cu alloy. *J. Alloys Compd.* **2021**, *867*, 158920. [\[CrossRef\]](#)
4. Wu, S.; Yin, J.; Luo, Y.; Huang, J.; Wang, Y.; Liu, Y.; Zhong, Y. A high strength Al–Zr alloy with good electrical conductivity by combining gas-assisted continuous casting and extrusion with subsequent thermomechanical treatment. *Mater. Today Commun.* **2023**, *37*, 107194. [\[CrossRef\]](#)
5. Ujah, C.O.; Kallon, D.V.V. Trends in Aluminium Matrix Composite Development. *Crystals* **2022**, *12*, 1357. [\[CrossRef\]](#)
6. Singla, A.; Singh, Y. Fabrication methods of nano-based metal matrix composites: A review. *AIP Conf. Proc.* **2023**, *2521*, 020025. [\[CrossRef\]](#)
7. Singh, H.; Singh, K.; Vardhan, S.; Mohan, S.; Singh, V. A comprehensive review of aluminium matrix composite reinforcement and fabrication methodologies. *Funct. Compos. Struct.* **2021**, *3*, 015007. [\[CrossRef\]](#)
8. Ma, K.; Lavernia, E.J.; Schoenung, J.M. Particulate Reinforced Aluminum Alloy Matrix Composites—A Review on the Effect of Microconstituents. *Rev. Adv. Mater. Sci.* **2017**, *48*, 91–104.
9. Prosviryakov, A.; Bazlov, A. The Study of Thermal Stability of Mechanically Alloyed Al-5 wt.% TiO<sub>2</sub> Composites with Cu and Stearic Acid Additives. *Appl. Sci.* **2023**, *13*, 1104. [\[CrossRef\]](#)
10. Prosviryakov, A.S.; Shcherbachev, K.D.; Tabachkova, N.Y. Investigation of nanostructured Al-10 wt.% Zr material prepared by ball milling for high temperature applications. *Mater. Charact.* **2017**, *123*, 173–177. [\[CrossRef\]](#)
11. Chak, V.; Chattopadhyay, H.; Dora, T.L. A review on fabrication methods, reinforcements and mechanical properties of aluminum matrix composites. *J. Manuf. Process.* **2020**, *56*, 1059–1074. [\[CrossRef\]](#)
12. Samal, P.; Vundavilli, P.R.; Meher, A.; Mahapatra, M.M. Recent progress in aluminum metal matrix composites: A review on processing, mechanical and wear properties. *J. Manuf. Process.* **2020**, *59*, 131–152. [\[CrossRef\]](#)
13. Heydari Vini, M.; Daneshmand, S.; Patra, I.; Lafta, H.A.; Jawad Kadhim, Z. Effect of Al<sub>2</sub>O<sub>3</sub> particles on the mechanical and wear properties of Al base composites. *Proc. Inst. Mech. Eng. Part C J. Mech. Eng. Sci.* **2023**, *237*, 3063–3072. [\[CrossRef\]](#)
14. Zhang, P.; Zhang, W.; Du, Y.; Wang, Y. High-performance Al-1.5 wt% Si–Al<sub>2</sub>O<sub>3</sub> composite by vortex-free high-speed stir casting. *J. Manuf.* **2020**, *56*, 1126–1135. [\[CrossRef\]](#)
15. Miserez, A.; Stucklin, S.; Rossoll, A.; San Marchi, C.; Mortensen, A. Influence of heat treatment and particle shape on mechanical properties of infiltrated Al<sub>2</sub>O<sub>3</sub> particle reinforced Al–2 wt% Cu. *Mater. Sci. Technol.* **2002**, *18*, 1461–1470. [\[CrossRef\]](#)
16. Travitzky, N.A. Effect of metal volume fraction on the mechanical properties of alumina/aluminum composites. *J. Mater. Sci.* **2001**, *36*, 4459–4463. [\[CrossRef\]](#)
17. Chak, V.; Chattopadhyay, H.; Shanu, C. A review on the employment of ultrasonic-assisted routes for synthesis of aluminum matrix composites. *Mater. Today Proc.* **2023**, *72*, 1170–1174. [\[CrossRef\]](#)
18. Zhukov, I.A.; Kozulin, A.A.; Khrustalyov, A.P.; Kahidze, N.I.; Khmeleva, M.G.; Moskvichev, E.N.; Lychagin, D.V.; Vorozhtsov, A.B. Pure Aluminum Structure and Mechanical Properties Modified by Al<sub>2</sub>O<sub>3</sub> Nanoparticles and Ultrasonic Treatment. *Metals* **2019**, *9*, 1199. [\[CrossRef\]](#)
19. Luan, B.F.; Wu, G.H.; Liu, W.; Hansen, N.; Lei, T. High strength Al<sub>2</sub>O<sub>3</sub>p/2024Al composites—Effect of particles, subgrains and precipitates. *Mater. Sci. Technol.* **2005**, *21*, 1440–1443. [\[CrossRef\]](#)
20. Qin, X.H.; Jiang, D.L.; Dong, S.M. Nanometer, submicron and micron sized aluminum powder prepared by semi-solid mechanical stirring method with addition of ceramic particles. *Mater. Sci. Eng. A* **2004**, *385*, 31–37. [\[CrossRef\]](#)

21. Çalışkan, O.; Sunar, T.; Özyürek, D. Mechanical and wear performance of A356/Al<sub>2</sub>O<sub>3</sub> aluminum nanocomposites by considering the mechanical milling time and microstructural properties. *Ind. Lubr. Tribol.* **2023**, *75*, 465–473. [[CrossRef](#)]
22. Prabhu, B.; Suryanarayana, C.; An, L.; Vaidyanathan, R. Synthesis and characterization of high volume fraction Al–Al<sub>2</sub>O<sub>3</sub> nanocomposite powders by high-energy milling. *Mater. Sci. Eng. A* **2006**, *425*, 192–200. [[CrossRef](#)]
23. Hernández Rivera, J.L.; Cruz Rivera, J.J.; Paz del Ángel, V.; Garibay Febles, V.; Coreño Alonso, O.; Martínez-Sánchez, R. Structural and morphological study of a 2024 Al–Al<sub>2</sub>O<sub>3</sub> composite produced by mechanical alloying in high energy mill. *Mater. Des.* **2012**, *37*, 96–101. [[CrossRef](#)]
24. Prashanth, M.; Karunanithi, R.; Mohideen, S.R.; Sivasankaran, S.; Vlahović, M. A comparative study on X-ray peak broadening analysis of mechanically alloyed Al<sub>2</sub>O<sub>3</sub> particles dispersion strengthened Al 7017 alloy. *Mater. Chem. Phys.* **2023**, *294*, 127015. [[CrossRef](#)]
25. Zebarjad, S.M.; Sajjadi, S.A. Microstructure evaluation of Al–Al<sub>2</sub>O<sub>3</sub> composite produced by mechanical alloying method. *Mater. Des.* **2006**, *27*, 684–688. [[CrossRef](#)]
26. Zebarjad, S.M.; Sajjadi, S.A. Dependency of physical and mechanical properties of mechanical alloyed Al–Al<sub>2</sub>O<sub>3</sub> composite on milling time. *Mater. Des.* **2007**, *28*, 2113–2120. [[CrossRef](#)]
27. Toozandehjani, M.; Matori, K.A.; Ostovan, F.; Abdul Aziz, S.; Mamat, M.S. Effect of Milling Time on the Microstructure, Physical and Mechanical Properties of Al–Al<sub>2</sub>O<sub>3</sub> Nanocomposite Synthesized by Ball Milling and Powder Metallurgy. *Materials* **2017**, *10*, 1232. [[CrossRef](#)]
28. Poirier, D.; Drew, R.A.L.; Trudeau, M.L.; Gauvin, R. Fabrication and properties of mechanically milled alumina/aluminum nanocomposites. *Mater. Sci. Eng. A* **2010**, *527*, 7605–7614. [[CrossRef](#)]
29. Wagih, A. Synthesis of Nanocrystalline Al<sub>2</sub>O<sub>3</sub> Reinforced Al Nanocomposites by High-Energy Mechanical Alloying: Microstructural Evolution and Mechanical Properties. *Trans. Indian. Inst. Met.* **2016**, *69*, 851–857. [[CrossRef](#)]
30. Tavoosi, M.; Karimzadeh, F.; Enayati, M.H. Wear behaviour of Al–Al<sub>2</sub>O<sub>3</sub> nanocomposites prepared by mechanical alloying and hot pressing. *Mater. Sci. Technol.* **2010**, *26*, 1114–1119. [[CrossRef](#)]
31. Razavi Tousi, S.S.; Yazdani Rad, R.; Salahi, E.; Mobasherpour, I.; Razavi, M. Production of Al–20 wt.% Al<sub>2</sub>O<sub>3</sub> composite powder using high energy milling. *Powder Technol.* **2009**, *192*, 346–351. [[CrossRef](#)]
32. Benjamin, J.S.; Volin, T.E. The Mechanism of Mechanical Alloying. *Metall. Trans.* **1974**, *5*, 1929–1934. [[CrossRef](#)]
33. Suryanarayana, C. Mechanical alloying: A critical review. *Mater. Res. Lett.* **2022**, *10*, 619–647. [[CrossRef](#)]
34. Suryanarayana, C. Mechanical Alloying and Milling. *Prog. Mater. Sci.* **2001**, *46*, 1–184. [[CrossRef](#)]
35. Suryanarayana, C.; Klassen, T.; Ivanov, E. Synthesis of nanocomposites and amorphous alloys by mechanical alloying. *J. Mater. Sci.* **2011**, *46*, 6301–6315. [[CrossRef](#)]
36. Zhang, D.L. Processing of advanced materials using high-energy mechanical milling. *Prog. Mater. Sci.* **2004**, *49*, 537–560. [[CrossRef](#)]
37. Shuai, C.; He, C.; Peng, S.; Qi, F.; Wang, G.; Min, A.; Yang, W.; Wang, W. Mechanical Alloying of Immiscible Metallic Systems: Process, Microstructure, and Mechanism. *Adv. Eng. Mater.* **2021**, *23*, 2001098. [[CrossRef](#)]
38. Jia, Z.; Hu, G.; Forbord, B.; Solberg, J.K. Enhancement of recrystallization resistance of Al–Zr–Mn by two-step precipitation annealing. *Mater. Sci. Eng. A* **2008**, *483–484*, 195–198. [[CrossRef](#)]
39. Al-Aqeeli, N.; Mendoza-Suarez, G.; Suryanarayana, C.; Drew, R.A.L. Development of new Al-based nanocomposites by mechanical alloying. *Mater. Sci. Eng. A* **2008**, *480*, 392–396. [[CrossRef](#)]
40. Muthaiah, V.M.S.; Mula, S. Effect of zirconium on thermal stability of nanocrystalline aluminum alloy prepared by mechanical alloying. *J. Alloys Compd.* **2016**, *688*, 571–580. [[CrossRef](#)]
41. Srinivasarao, B.; Suryanarayana, C.; Oh-ishi, K.; Hono, K. Microstructure and mechanical properties of Al–Zr nanocomposite materials. *Mater. Sci. Eng. A* **2009**, *518*, 100–107. [[CrossRef](#)]
42. Prosviryakov, A.S.; Shcherbachev, K.D. Strengthening of mechanically alloyed Al-based alloy with high Zr contents. *Mater. Sci. Eng. A* **2018**, *713*, 174–179. [[CrossRef](#)]
43. Kaveendran, B.; Wang, G.S.; Huang, L.J.; Geng, L.; Peng, H.X. In situ (Al<sub>3</sub>Zr + Al<sub>2</sub>O<sub>3np</sub>)/2024Al metal matrix composite with novel reinforcement distributions fabricated by reaction hot pressing. *J. Alloys Compd.* **2013**, *581*, 16–22. [[CrossRef](#)]
44. Mikhaylovskaya, A.V.; Kotov, A.D.; Kishchik, M.S.; Prosviryakov, A.S.; Portnoy, V.K. The Effect of Isothermal Multi-Directional Forging on the Grain Structure, Superplasticity, and Mechanical Properties of the Conventional Al–Mg-Based Alloy. *Metals* **2019**, *9*, 33. [[CrossRef](#)]
45. Nelson, J.B.; Riley, D.P. An experimental investigation of extrapolation methods in the derivation of accurate unit-cell dimensions of crystals. *Proc. Phys. Soc.* **1945**, *57*, 160–177. [[CrossRef](#)]
46. Belov, N.A. Aluminum casting alloys with high content of zirconium. *Mater. Sci. Forum* **1996**, *217–222*, 293–298. [[CrossRef](#)]
47. Prosviryakov, A.S.; Shcherbachev, K.D.; Tabachkova, N.Y. Microstructural characterization of mechanically alloyed Al–Cu–Mn alloy with zirconium. *Mater. Sci. Eng. A* **2015**, *623*, 109–113. [[CrossRef](#)]
48. Williamson, G.K.; Hall, W.H. X-ray line broadening from filed aluminum and wolfram. *Acta Metall.* **1953**, *1*, 22–31. [[CrossRef](#)]
49. Shanmugasundaram, T.; Heilmaier, M.; Murty, B.S.; Subramanya Sarma, V. Microstructure and Mechanical Properties of Nanostructured Al-4Cu Alloy Produced by Mechanical Alloying and Vacuum Hot Pressing. *Metall. Mater. Trans. A* **2009**, *40*, 2798–2801. [[CrossRef](#)]

50. Williamson, G.K.; Smallman, R.E. Dislocation densities in some annealed and cold-worked metals from measurements on the X-ray Debye-Scherrer spectrum. *Philos. Mag.* **1956**, *1*, 34–46. [[CrossRef](#)]
51. Akbarpour, M.R.; Salahi, E.; Alikhani Hesari, F.; Simchi, A.; Kim, H.S. Fabrication, characterization and mechanical properties of hybrid composites of copper using the nanoparticulates of SiC and carbon nanotubes. *Mater. Sci. Eng. A* **2013**, *572*, 83–90. [[CrossRef](#)]
52. Mohammadi, A.; Enikeev, N.A.; Murashkin, M.Y.; Arita, M.; Edalati, K. Examination of inverse Hall-Petch relation in nanostructured aluminum alloys by ultra-severe plastic deformation. *J. Mater. Sci. Technol.* **2021**, *91*, 78–89. [[CrossRef](#)]
53. Meyers, M.A.; Mishra, A.; Benson, D.J. Mechanical properties of nanocrystalline materials. *Prog. Mater. Sci.* **2006**, *51*, 427–556. [[CrossRef](#)]

**Disclaimer/Publisher’s Note:** The statements, opinions and data contained in all publications are solely those of the individual author(s) and contributor(s) and not of MDPI and/or the editor(s). MDPI and/or the editor(s) disclaim responsibility for any injury to people or property resulting from any ideas, methods, instructions or products referred to in the content.